Monthly Notices
of the
ROYAL ASTRONOMICAL SOCIETY
MNRAS **454,** 1260–1265 (2015) doi:10.1093/mnras/stv2171

# Discovery of two gravitationally lensed quasars in the Dark Energy Survey

A. Agnello,[1⋆] T. Treu,[1⋆†] F. Ostrovski,[2,3,4] P. L. Schechter,[5] E. J. Buckley-Geer,[6] H. Lin,[6] M. W. Auger,[2] F. Courbin,[7] C. D. Fassnacht,[8] J. Frieman,[6] N. Kuropatkin,[6] P. J. Marshall,[9] R. G. McMahon,[2,3] G. Meylan,[7] A. More,[10] S. H. Suyu,[11] C. E. Rusu,[8] D. Finley,[6] T. Abbott,[12] F. B. Abdalla,[13] S. Allam,[6] J. Annis,[6] M. Banerji,[2,3] A. Benoit-Lévy,[13] E. Bertin,[14,15] D. Brooks,[13] D. L. Burke,[9,16] A. Carnero Rosell,[17,18] M. Carrasco Kind,[19,20] J. Carretero,[21,22] C. E. Cunha,[16] C. B. D'Andrea,[23] L. N. da Costa,[17,18] S. Desai,[24,25] H. T. Diehl,[6] J. P. Dietrich,[24,25] P. Doel,[13] T. F. Eifler,[26,27] J. Estrada,[6] A. Fausti Neto,[17] B. Flaugher,[6] P. Fosalba,[21] D. W. Gerdes,[28] D. Gruen,[29,30] G. Gutierrez,[6] K. Honscheid,[31,32] D. J. James,[12] K. Kuehn,[33] O. Lahav,[13] M. Lima,[17,34] M. A. G. Maia,[17,18] M. March,[26] J. L. Marshall,[35] P. Martini,[31,32] P. Melchior,[31,32] C. J. Miller,[28,36] R. Miquel,[22,37] R. C. Nichol,[23] R. Ogando,[17,18] A. A. Plazas,[27] K. Reil,[9] A. K. Romer,[38] A. Roodman,[9,16] M. Sako,[26] E. Sanchez,[39] B. Santiago,[17,40] V. Scarpine,[6] M. Schubnell,[28] I. Sevilla-Noarbe,[19,39] R. C. Smith,[12] M. Soares-Santos,[6] F. Sobreira,[6,17] E. Suchyta,[31,32] M. E. C. Swanson,[20] G. Tarle,[28] J. Thaler,[19] D. Tucker,[6] A. R. Walker,[12] R. H. Wechsler[9,16,41] and Y. Zhang[28]

*Affiliations are listed at the end of the paper*

Accepted 2015 August 26. Received 2015 August 26; in original form 2015 August 4

## ABSTRACT

We present spectroscopic confirmation of two new gravitationally lensed quasars, discovered in the Dark Energy Survey (DES) and *Wide-field Infrared Survey Explorer* (*WISE*) based on their multiband photometry and extended morphology in DES images. Images of DES J0115−5244 show a red galaxy with two blue point sources at either side, which are images of the same quasar at $z_s = 1.64$ as obtained by our long-slit spectroscopic data. The Einstein radius estimated from the DES images is 0.51 arcsec. DES J2146−0047 is in the area of overlap between DES and the Sloan Digital Sky Survey (SDSS). Two blue components are visible in the DES and SDSS images. The SDSS fibre spectrum shows a quasar component at $z_s = 2.38$ and absorption by Mg II and Fe II at $z_l = 0.799$, which we tentatively associate with the foreground lens galaxy. Our long-slit spectra show that the blue components are resolved images of the same quasar. The Einstein radius is 0.68 arcsec, corresponding to an enclosed mass of $1.6 \times 10^{11}\,M_\odot$. Three other candidates were observed and rejected, two being low-redshift pairs of starburst galaxies, and one being a quasar behind a blue star. These first confirmation results provide an important empirical validation of the data mining and model-based selection that is being applied to the entire DES data set.

**Key words:** gravitational lensing: strong – methods: observational – methods: statistical – quasars: emission lines.

## 1 INTRODUCTION

Gravitationally lensed quasars provide unique insights into a variety of fundamental open problems in cosmology and extragalactic

⋆ E-mail: aagnello@astro.ucla.edu (AA); tt@astro.ucla.edu (TT)
† Packard Fellow.

astrophysics (e.g. Courbin, Saha & Schechter 2002). When a quasar is strongly lensed by a galaxy, it results in multiple images of the same source, accompanied by arcs or rings that map the lensed host of the quasar. The light curves of different images are offset by a measurable time delay (e.g. Schechter et al. 1997; Tewes et al. 2013) that depends on the cosmological distances to the lens and the source and the gravitational potential of the lens (Refsdal 1964). This enables one-step measurements of the expansion history of the Universe and the dark matter haloes of the massive galaxies that act as deflectors (e.g. Suyu et al. 2014). The microlensing effect on the multiple quasar images, induced by stars in the deflector, provides a quantitative handle on the stellar content of the lens galaxies (e.g. Schechter & Wambsganss 2002; Oguri, Rusu & Falco 2014; Schechter et al. 2014; Jiménez-Vicente et al. 2015), and can simultaneously provide constraints on the inner structure of the lensed quasar, both the accretion disc size and the thermal profile (e.g. Anguita et al. 2008; Eigenbrod et al. 2008; Poindexter, Morgan & Kochanek 2008; Motta et al. 2012) as well as the geometry of the broad line region (e.g. Sluse et al. 2011; Guerras et al. 2013; Braibant et al. 2014). Furthermore, millilensing via the so-called flux ratio anomalies provides a unique probe of the mass function of substructure and thus ultimately of the nature of dark matter (Mao & Schneider 1998; Metcalf & Madau 2001; Dalal & Kochanek 2002; Metcalf 2002; Nierenberg et al. 2014). Finally, source reconstruction of the lensed quasar and its host give a direct view of quasar-host coevolution up to $z \sim 2$ (Peng et al. 2006; Rusu et al. 2015).

Advancement in the field is currently limited by the paucity of known systems suitable for detailed follow-up and analysis. A large sample of new systems will be transformative. To accomplish this, the STRIDES project,[1] a broad external collaboration of the Dark Energy Survey[2] (DES, http://www.darkenergysurvey.org/index.shtml), aims at the discovery of the ∼100 lensed quasars with primary image brighter than $i = 21$ mag predicted by Oguri & Marshall (2010) to lie within the DES footprint.

The identification of such rare systems over 5000 deg$^2$ of DES imaging data is a classic needle-in-a-haystack problem. The challenge is possibly greater than that faced in the SDSS data set (Oguri et al. 2006; Inada et al. 2008), as DES catalogues do not contain *u*-band data and there is no built-in spectroscopic data set to aid in the quasar selection. Fortunately, the DES image quality (median seeing ∼0.9 arcsec) is better than that of SDSS, so one can rely on more accurate morphological information for candidate selection. New techniques have been developed in order to address this challenge (Agnello et al. 2015; Chan et al. 2015).

Here, we report on the first spectroscopic confirmation of lensed quasars from DES. We have obtained spectra of five of the 68 high-grade, small-separation candidate lensed quasars in the Year-1 DES data release footprint (hereafter Y1A1; Diehl et al. 2014), covering ≈1200 deg$^2$ in the Southern hemisphere.

This *Letter* is organized as follows. Section 2 briefly illustrates the candidate-selection process and DES images of the two successful candidates from the first spectroscopic follow-up. Section 3 shows the long-slit spectroscopic data obtained for these systems. In Section 4, we present the lensing properties that can be inferred with current data and conclude in Section 5. Throughout this Letter, DES and *WISE* magnitudes are in the AB and Vega system, respectively. When needed in Section 4, we adopt a concordance cosmology with $\Omega_m = 0.3$, $\Omega_\Lambda = 0.7$, $H_0 = 70\,\mathrm{km\,s^{-1}\,Mpc^{-1}}$.

[1] STRong lensing Insight in the Dark Energy Survey, PI Treu, full list of Co-PIs and Co-Is at http://strides.physics.ucsb.edu.

[2] See Flaugher et al. (2015) for the technical setup of the Dark Energy Camera.

## 2 QUASAR LENS CANDIDATE SELECTION

We selected small-separation candidates from the DES Y1A1 data release, using a combination of colour cuts and data mining and model-based selection. Following Agnello et al. (2015), we adopt a multistep strategy, whereby *targets* are first selected from catalogue data, and *candidates* are then selected from the targets by analysis of the actual multiband images. This multistep procedure allows one to keep the problem computationally fast.

### 2.1 Preselection

Objects are preselected in the DES catalogue based on their 'blue' colours and extended morphology. The colour selection, satisfying

$$g - r < 0.6,\ r - i < 0.45,\ i - z < 0.55,$$
$$2.5 < i - W1 < 5.5,\ 0.7 < W1 - W2 < 2.0,$$
$$g - i < 1.2(i - W1) - 2.8\,, \quad (1)$$

is only used to exclude the majority of galaxies and nearby blue stars from the pool being examined. Of these, we retain those satisfying

$$\texttt{psf\_mag} - \texttt{model\_mag} \geq \mathrm{dmag} \quad (2)$$

in DES *g*, *r*, *i* bands simultaneously, with dmag = 0.125 in *g*, *r* bands and 0.2 in the *i* band. This ensures that the objects are not point-like (cf. Reed et al. 2015, who use a similar but converse criterion for point-like objects).

Out of ∼$2 \times 10^5$ 'blue' systems, extended in the *i* band and with acceptable colours in DES *g*, *r*, *i*, *z* and *WISE* *W*1, *W*2 magnitudes, ∼4000 are brighter than limiting magnitudes $i = 21$ or $W1 = 17$ and extended also in *g*, *r* bands.

### 2.2 Targets

Of the 4000 blue extended objects, targets are selected by neural network classifiers (ANNs) based on their photometry and multiband morphology obtained at catalogue level. In particular, DES `model` *g*, *r*, *i*, *z* magnitudes and *WISE* `w1mpro` (*W*1), `w2mpro` (*W*2) magnitudes are used for the photometry and DES model position angles and axis ratios in *g*, *r*, *i*, *z* are used for the morphology. ANNs produce membership probabilities for each object to belong to different classes, from which the targets are selected with cuts in output probabilities. The full procedure is discussed in detail by Agnello et al. (2015). ANNs relying just on the photometry select 430 targets, out of which 136 are also selected by ANNs relying on multiband morphologies as well.

### 2.3 Candidates

The DES *g*, *r*, *i*, *z*, *Y* image cutouts of selected targets have been modelled as combinations of point sources and galaxies to extract the SEDs of the extended and point sources. Based on the model results, we ranked candidates from '0' (not a lens) to '3' (good lens candidate), based on whether: (i) the point sources have consistent SEDs at least in *r*, *i*, *z* bands; (ii) their SEDs are compatible with those of quasars; (iii) the fainter quasar image is also redder in $g - r$; (iv) a possible lens galaxy is detected in the residuals or in *Y* band.

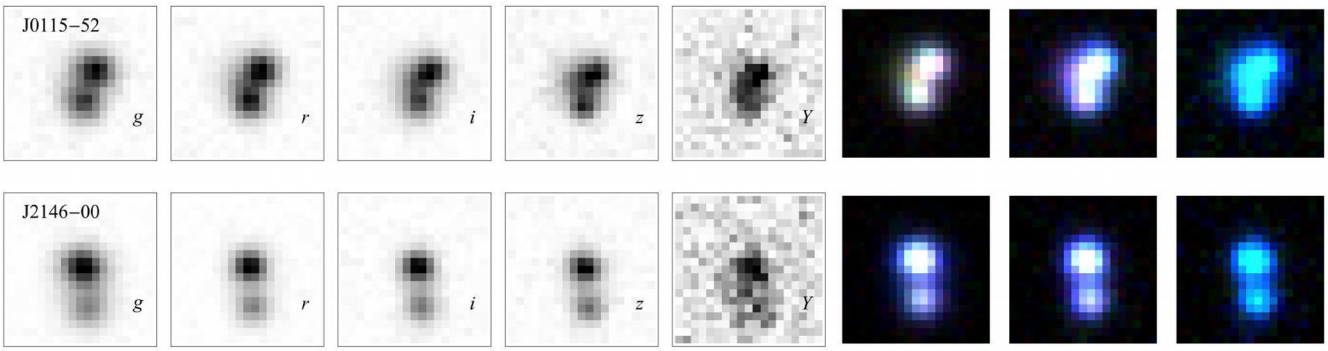


**Figure 1.** DES multiband single-epoch images with best seeing of DES J0115−5244 (top) and DES J2146−0047 (bottom), in 5 arcsec × 5 arcsec cutouts. North is up and east is left. From left to right, DES *g*, *r*, *i*, *z*, *Y*, and colour composites in *gri*, *riz*, *izY*.

**Table 1.** Measured parameters of the systems in this Letter. The redshift of source $z_s$ and lens $z_l$ are obtained from our long-slit spectra and the SDSS public data. The relative astrometry and magnitudes of brighter (A) and fainter (B) quasar image and lens galaxy (G) are obtained by modelling the single-epoch DES images with best image quality (quoted under 'seeing FWHM'). The right ascension (resp. declination) increases to the E (resp. to the N). Upper limits are given for magnitudes with ≥0.33 uncertainty. The galaxy in DES J2146−0047 is above the detection limit in DES *Y* band and in CFHT *i*, *z* bands. All quoted errors account for statistical uncertainties from cutout fitting an not e.g. possible systematics from PSF mismatch.

| Syst. | $z_s$ | $z_l$ | ΔRA (arcsec) | ΔDec. (arcsec) | *g* | *r* | *i* | *z* | *Y* |
|---|---|---|---|---|---|---|---|---|---|
| DES J0115−5244 | 1.64 | – | | | | | | | |
| A | – | – | 0.00 | 0.00 | 20.82 ± 0.08 | 19.97 ± 0.10 | 19.91 ± 0.10 | 20.01 ± 0.15 | 19.45 ± 0.14 |
| B | – | – | 0.36 ± 0.02 | 0.97 ± 0.02 | 21.12 ± 0.07 | 20.21 ± 0.08 | 20.06 ± 0.10 | 20.21 ± 0.11 | 19.58 ± 0.09 |
| G | – | – | 0.73 ± 0.05 | 0.22 ± 0.05 | >22.66 | 21.35 ± 0.28 | 20.62 ± 0.16 | 20.22 ± 0.13 | 19.59 ± 0.21 |
| Seeing FWHM | – | – | – | – | 1.00 arcsec | 0.98 arcsec | 0.90 arcsec | 0.76 arcsec | 0.75 arcsec |
| DES `model` | – | – | – | – | 19.95 | 19.48 | 19.10 | 18.89 | 18.73 |
| DES J2146−0047 | 2.38 | 0.799 | | | | | | | |
| A | – | – | 0.00 | 0.00 | 19.93 ± 0.13 | 19.85 ± 0.15 | 19.92 ± 0.16 | 19.88 ± 0.16 | 20.23 ± 0.15 |
| B | – | – | −0.17 ± 0.03 | −1.35 ± 0.03 | 20.88 ± 0.14 | 20.50 ± 0.15 | 20.39 ± 0.15 | 20.47 ± 0.15 | 20.71 ± 0.18 |
| G | – | – | 0.17 ± 0.05 | −0.70 ± 0.05 | – | – | – | – | 20.75 ± 0.30 |
| G (CFHT) | – | – | −0.1008 ± 0.05 | −0.76 ± 0.05 | – | – | 21.04 ± 0.05 | 20.51 ± 0.05 | – |
| Seeing FWHM | – | – | – | – | 1.12 arcsec | 0.87 arcsec | 0.82 arcsec | 0.77 arcsec | 1.26 arcsec |
| DES `model` | – | – | – | – | 19.52 | 19.67 | 19.48 | 19.16 | 19.05 |

At this stage, the selection shifts from automatic procedures (pre-selection, ANNs, modelling) to the investigator discretion, even though the ranking is based on the four quantitative criteria listed above. The final sample has 23 grade-'3' candidates and 45, 51, 17 with grades '2', '1', '0', respectively.

### 2.4 First two confirmed lenses

Fig. 1 shows DES multiband, single-epoch images in the best seeing conditions of the two successful candidates for which we describe spectroscopic follow-up in the next section. They are DES J0115−5244 at 01:15:57.32 −52:44:23.20 (top) and DES J2146−0047 at 21:46:46.04 −00:47:44.3 (bottom).

The photometry and relative astrometry of the components in our composite models are summarized in Table 1. We have used the single-epoch DES cutouts with best image quality and adopted DES models of the PSF from nearby stars. For DES J2146−0047, we also fit Moffat profiles with the same structural parameters to each quasar image and a Sérsic profile to the lensing galaxy in archival Canada–France–Hawaii Telescope (CFHT) MegaCam *i*, *z*-band images (Programme 10BC22, PI: van Waerbeke). The resulting photometry is given in Table 1 below the DES one. Even though the galaxy is below the detection limit in DES single-epoch data except in the *Y* band, it is securely detected in CFHT data in *i*, *z* bands as well.

Three additional candidates have been observed during the same observing run and ruled out as lensed quasars. They are briefly described in Section 3.3 below.

## 3 SPECTROSCOPIC CONFIRMATION

Spectra were obtained with the Inamori Magellan Areal Camera and Spectrograph (IMACS; Dressler et al. 2011) on the Baade 6.5-m telescope on UT 2015 June 19. The f/4 camera was used with 0.70 − arcsec slit mask. The data were binned factors of 2 along the slit, giving a scale of 0.22 arcsec pixel$^{-1}$, and 4 in the spectral direction, which combined with a 300 l mm$^{-1}$ grating gave a dispersion of 2.92 Å pixel$^{-1}$. Two CCDs covered the spectra over 3770–5260 Å and 5350–6880 Å. The seeing ranged between 0.8 and 1.2 arcsec, and all our candidates were partially or completely resolved. Two spectra of 600 s were taken for each object. The data were reduced using standard IRAF routines.

One-dimensional (1D) spectra have been extracted by modelling the 2D spectra as superpositions of Gaussian tracks in the spatial dimension, one per component, having peak positions $(p_1, p_2)$ that are linear functions of the wavelength with the same slope ($\mathrm{d}p/\mathrm{d}\lambda$). Even though the individual tracks are generally well separated, this procedure ensures that the resulting 1D spectra are as independent as possible from one another and exploit all the information available in the 2D tracks.

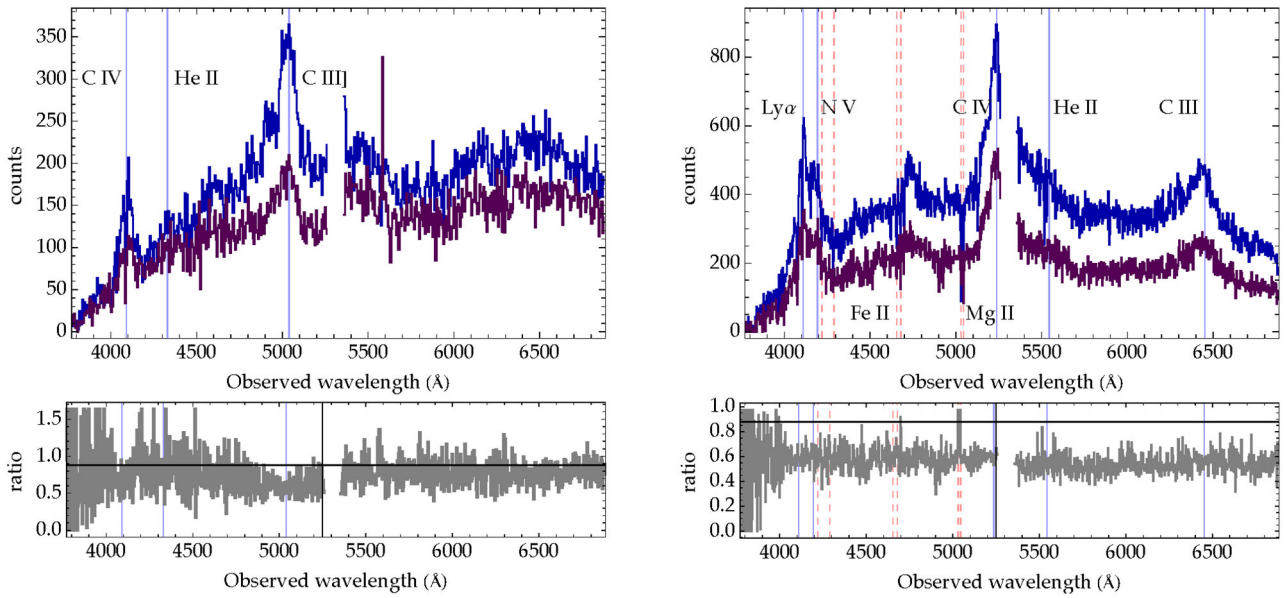


**Figure 2.** 1D sky-subtracted spectra of DES J0115−5244 (left) and DES J2146−0047 (right). The red and blue histograms show the spectra of the two components, demonstrating that they are images of the same quasar. Emission and absorption lines are marked by blue (solid) and red (dashed) vertical lines, respectively.

Five grade-'3' candidates were visible and observed. The resulting spectra are described below. The results on the two confirmed lenses are shown in Fig. 2.

### 3.1 DES J0115−5244

The 1D spectra of DES J0115−5244 show the same broad emission lines (C IV, He II, C III]) at $z_s = 1.64$, with a uniform ratio between the two spectra in the red, as shown in Fig. 2, indicating that the low-order differences between the two spectra are due to differential reddening, or perhaps chromatic microlensing. Together with the presence of a red galaxy in the DES images, the spectra confirm DES J0115−5244 as a strongly lensed quasar, with image separation ≈1.04 arcsec. Unfortunately, the S/N ratio is too low to securely detect stellar absorption lines from the deflector.

### 3.2 DES J2146−0047

The 1D spectra of DES J2146−0047 show two components with the same broad emission lines at $z_s = 2.38$, consistent with the public SDSS fibre spectrum. Prominent Mg II and Fe II absorption lines at $z_l = 0.799$ are detected in both spectra (Fig. 2). The ratio between the two spectra is constant, which together with the detection of a galaxy in *izY* bands confirms DES J2146−0047 as a strongly lensed quasar, with image separation ≈1.32 arcsec. We associate the lens redshift with the galaxy responsible for the absorption lines at $z_l$. This system has been independently identified as part of the SDSS-III quasar lens sample (More et al., in preparation).

### 3.3 False positives

Two candidates, at 20:53:56.5 −56:09:36 and 22:17:52.5 −53:57:15, respectively, are pairs of compact, star-forming galaxies. The third rejected candidate, at 22:00:24.11 +01:10:37.56, is an alignment of a $z = 1.37$ red quasar and a blue star, with the same $r - i$ and $i - z$ colours by coincidence.

In general, pairs of compact star forming galaxies at $z \approx 0.2$–0.3 are the main residual contaminant from the candidate-selection procedure, because their broad-band colours are consistent with those of quasars. This includes initial candidates that we rejected based on their available SDSS spectra. In *WISE* magnitudes, they tend to lie at $W2 > 14$ and $W1 - W2 < 0.8$, across the limiting locus of Assef et al. (2013), a region that however is occupied also by spectroscopicallyconfirmed quasars and some of the candidates from this search.

## 4 LENSING PROPERTIES

Even though the current data are not sufficient for a detailed lensing model, they can be used to derive simple properties of the lens galaxies. To this aim, we adopt a Singular Isothermal Sphere (SIS) model for the mass density profile of the deflector, which is commonly considered the simplest model apt to describe galaxy-scale lenses (Treu 2010). The SIS projected surface density is

$$\Sigma(R) = \frac{1}{2}\Sigma_{cr}(R/R_{\rm E})^{-1} \quad (3)$$

with $\Sigma_{\rm cr} = c^2 D_{\rm s}/(4\pi G D_{\rm l} D_{\rm ls})$ in terms of angular diameter distances to the source ($D_{\rm s}$), to the lens ($D_{\rm l}$) and between lens and source ($D_{\rm ls}$), and the Einstein radius $R_{\rm E}$ is defined such that it encloses a projected mass

$$M_{\rm E} = \pi \Sigma_{\rm cr} R_{\rm E}^2 . \quad (4)$$

The expected line-of-sight velocity dispersion of stars in the lens galaxy can be estimated via

$$\sigma_{\rm sis}^2 = \frac{c^2 R_{\rm E} D_{\rm s}}{4\pi D_{\rm l} D_{\rm ls}} . \quad (5)$$

Finally, neglecting microlensing, the total magnification of the point source can be estimated from the flux ratio $f_B/f_A$ as

$$\mu_{\rm tot} = 2\frac{1 + f_B/f_A}{1 - f_B/f_A} , \quad (6)$$

**Table 2.** Estimated lensing parameters and properties of the lens galaxy: Einstein radius $R_E$ (in angular units) and total magnification $\mu_{tot,\,i}$ from the fit to the quasar image positions and fluxes; magnification $\mu_{tot,\,c}$ on the quasar continua, from the 1D spectra; and SIS velocity dipersion $\sigma_{sis}$ and enclosed mass $M_E$ from the measured redshifts. For DES J0115−5244, $\sigma_{sis}$ and $M_E$ are under the hypothesis that the lens is midway between observer and source (i.e. $z_l = 0.635$).

| | DES J0115−5244 | DES J2146−0047 |
|---|---|---|
| $R_E$ | 0.513 arcsec | 0.680 arcsec |
| $\mu_{tot,\,i}$ | $26.0 \pm 20.0$ | $8.4 \pm 3.2$ |
| $\mu_{tot,\,c}$ | $16.0 \pm 13.0$ | $6.6 \pm 1.4$ |
| $\sigma_{sis}$ (km/s) | 190 | 215 |
| $M_E$ ($M_\odot$) | $0.95 \times 10^{11}$ | $1.6 \times 10^{11}$ |

where A is the brighter quasar image. Then, from Table 1 and confirmation spectra, we can estimate $R_E$, $M_E$, $\sigma_{sis}$ and $\mu_{tot}$. The Einstein radius is approximated by half the image separation (an exact result for SIS profiles). For the flux ratio, we use the average between *i* and *z* bands, for which the photometric fit is more robust against PSF mismatch and signal-to-noise ratio(S/N), and the effects of dust and microlensing are minimized. The results are summarized in Table 2. For DES J0115−5244, we adopted a lens redshift $z_l = 0.635$, which minimizes the critical surface density $\Sigma_{cr}$ and yields a lower bound on $\sigma_{sis}$. We also list the magnification inferred from the ratio of continua in the spectra around 6000 Å. With the positional uncertainties from Table 1, the relative uncertainty on $R_E$ is 1 per cent. With current data, the uncertainties on the magnifications are of the same order as their average value.

## 5 CONCLUSIONS

We have presented the very first results of a campaign to extend the known samples of lensed quasars by exploiting the large footprint of wide-field photometric surveys. In particular, we have spectroscopically confirmed two new systems, found in the DES Y1A1 release with data-mining techniques. Two additional candidates were ruled out by spectroscopic observations as pairs of $z \approx 0.2$ compact, narrow-line galaxies. Another candidate was ruled out as an alignment of a quasar and a blue star. The basic characteristics of the two confirmed systems are as follows.

*DES J0115−5244.* Consists of two images of a quasar at $z_s = 1.64$ lensed by a foreground galaxy visible in the DES images. No redshift is available for the lens galaxy. The Einstein Radius is estimated to be 0.51 arcsec.

*DES J2146−0047.* Consists of two images of a quasar at $z_s = 2.38$, with prominent Mg II absorption at $z_l = 0.799$, which we tentatively associate with the lens galaxy redshift. The redshift of the lensing galaxy is not confirmed in the spectroscopic follow-up by More et al. (in preparation), since detection of the Mg II and Fe II lines depends on S/N ratio and in fact is less evident in the worse of our two exposures, where track deconvolution becomes more noisy. Thus, deeper spectroscopic data will be needed to measure the redshift of the deflector, possibly based on stellar absorption lines. The Einstein Radius is estimated to be 0.68 arcsec.

The main class of contaminants (including candidates rejected based on their SDSS spectra) consists of groups of compact, star-forming galaxies at $z \sim 0.2$–$0.3$, because of their broad-band colours and compact morphology. With the observed sample, a strict cut in *WISE* $W1 - W2$ versus $W2$ would give a 100 per cent success rate, which drops at 40 per cent when the cut is relaxed. Still, with just five systems currently at hand, we would rather caution against these simple estimates.

Our search has delivered over 100 additional candidates from the Y1A1 data – and we expect many more from the next seasons of DES data. The results of this first follow-up effort are encouraging. However, a systematic follow-up campaign is needed to confirm large numbers of candidates, assess the purity of our selection technique, and carry out the many scientific investigations enabled by lensed quasars.

## ACKNOWLEDGEMENTS

This Letter includes data gathered with the 6.5m Baade Telescopes located at Las Campanas Observatory, Chile. AA, TT, CDF and CER acknowledge support from NSF grants AST-1312329 and AST-1450141 'Collaborative Research: Accurate cosmology with strong gravitational lens time delays'. AA and TT gratefully acknowledge support by the Packard Foundation through a Packard Research Fellowship to TT. SHS acknowledges support from the Ministry of Science and Technology in Taiwan via grant MOST-103-2112-M-001-003-MY3. FC and GM are supported by the Swiss National Science Foundation (SNSF). The work of PJM was supported by the US Department of Energy under contract number DE-AC02-76SF00515. We thank Tamara Davis, Cristina Furlanetto, Gary Bernstein and Tom Collett for useful comments on earlier versions of this Letter.

This Letter has gone through internal review by the DES collaboration. Funding for the DES Projects has been provided by the DOE and NSF (USA), MISE (Spain), STFC (UK), HEFCE (UK). NCSA (UIUC), KICP (U. Chicago), CCAPP (Ohio State), MIFPA (Texas A&M), CNPQ, FAPERJ, FINEP (Brazil), MINECO (Spain), DFG (Germany) and the Collaborating Institutions in the Dark Energy Survey. The Collaborating Institutions are Argonne Lab, UC Santa Cruz, University of Cambridge, CIEMAT-Madrid, University of Chicago, University College London, DES-Brazil Consortium, University of Edinburgh, ETH Zürich, Fermilab, University of Illinois, ICE (IEEC-CSIC), IFAE Barcelona, Lawrence Berkeley Lab, LMU München and the associated Excellence Cluster Universe, University of Michigan, NOAO, University of Nottingham, Ohio State University, University of Pennsylvania, University of Portsmouth, SLAC National Lab, Stanford University, University of Sussex, and Texas A&M University. The DES Data Management System is supported by the NSF under grant number AST-1138766. The DES participants from Spanish institutions are partially supported by MINECO under grants AYA2012-39559, ESP2013-48274, FPA2013-47986 and Centro de Excelencia Severo Ochoa SEV-2012-0234. Research leading to these results has received funding from the ERC under the EU's 7th Framework Programme including grants ERC 240672, 291329 and 306478.

## REFERENCES

Agnello A., Kelly B. C., Treu T., Marshall P. J., 2015, MNRAS, 448, 1446
Anguita T., Schmidt R. W., Turner E. L., Wambsganss J., Webster R. L., Loomis K. A., Long D., McMillan R., 2008, A&A, 480, 327
Assef R. J. et al., 2013, ApJ, 772, 26
Braibant L., Hutsemékers D., Sluse D., Anguita T., García-Vergara C. J., 2014, A&A, 565, L11
Chan J. H. H., Suyu S. H., Chiueh T., More A., Marshall P. J., Coupon J., Oguri M., Price P., 2015, ApJ, 807, 138
Courbin F., Saha P., Schechter P. L., 2002, 608, 1
Dalal N., Kochanek C. S., 2002, ApJ, 572, 25

Diehl H. T. et al., 2014, in Peck A. B., Benn C. R., Seaman R. L., eds, Proc. SPIE Conf. Ser. Vol. 9149, The Dark Energy Survey and operations: Year 1. SPIE, Bellingham, p. 91490V
Dressler A. et al., 2011, PASP, 123, 288
Eigenbrod A., Courbin F., Meylan G., Agol E., Anguita T., Schmidt R. W., Wambsganss J., 2008, A&A, 490, 933
Flaugher B. et al., 2015, preprint (arXiv:e-prints)
Guerras E., Mediavilla E., Jimenez-Vicente J., Kochanek C. S., Muñoz J. A., Falco E., Motta V., 2013, ApJ, 764, 160
Inada N. et al., 2008, AJ, 135, 496
Jiménez-Vicente J., Mediavilla E., Kochanek C. S., Muñoz J. A., 2015, ApJ, 799, 149
Mao S., Schneider P., 1998, MNRAS, 295, 587
Metcalf R. B., 2002, ApJ, 580, 696
Metcalf R. B., Madau P., 2001, ApJ, 563, 9
Motta V., Mediavilla E., Falco E., Muñoz J. A., 2012, ApJ, 755, 82
Nierenberg A. M., Treu T., Wright S. A., Fassnacht C. D., Auger M. W., 2014, MNRAS, 442, 2434
Oguri M., Marshall P. J., 2010, MNRAS, 405, 2579
Oguri M. et al., 2006, AJ, 132, 999
Oguri M., Rusu C. E., Falco E. E., 2014, MNRAS, 439, 2494
Peng C. Y., Impey C. D., Rix H.-W., Kochanek C. S., Keeton C. R., Falco E. E., Lehár J., McLeod B. A., 2006, ApJ, 649, 616
Poindexter S., Morgan N., Kochanek C. S., 2008, ApJ, 673, 34
Reed S. L. et al., 2015, preprint (arXiv:e-prints)
Refsdal S., 1964, MNRAS, 128, 307
Rusu C. E. et al., 2015, preprint (arXiv:e-prints)
Schechter P. L., Wambsganss J., 2002, ApJ, 580, 685
Schechter P. L. et al., 1997, ApJ, 475, L85
Schechter P. L., Pooley D., Blackburne J. A., Wambsganss J., 2014, ApJ, 793, 96
Sluse D. et al., 2011, A&A, 528, A100
Suyu S. H. et al., 2014, ApJ, 788, L35
Tewes M. et al., 2013, A&A, 556, A22
Treu T., 2010, ARA&A, 48, 87

[1]*Department of Physics and Astronomy, PAB, 430 Portola Plaza, Box 951547, Los Angeles, CA 90095-1547, USA*
[2]*Institute of Astronomy, Madingley Road, Cambridge CB3 0HA, UK*
[3]*Kavli Institute for Cosmology, University of Cambridge, Madingley Road, Cambridge CB3 0HA, UK*
[4]*CAPES Foundation, Ministry of Education of Brazil, Brasília, DF 70040-020, Brazil*
[5]*MIT Kavli Institute for Astrophysics and Space Research, 37-664G, 77 Massachusetts Avenue, Cambridge, MA 02139, USA*
[6]*Fermi National Accelerator Laboratory, Batavia, IL 60510, USA*
[7]*Laboratoire d'Astrophysique, Ecole Polytechnique Fédérale de Lausanne (EPFL), Observatoire de Sauverny, CH-1290 Versoix, Switzerland*
[8]*Department of Physics, University of California Davis, 1 Shields Avenue, Davis, CA 95616, USA*
[9]*Kavli Institute for Particle Astrophysics and Cosmology, Stanford University, 452 Lomita Mall, Stanford, CA 94035, USA*
[10]*Kavli IPMU (WPI), UTIAS, The University of Tokyo, Kashiwa, Chiba 277-8583, Japan*
[11]*Institute of Astronomy and Astrophysics, Academia Sinica, P.O. Box 23-141, Taipei 10617, Taiwan*
[12]*Cerro Tololo Inter-American Observatory, National Optical Astronomy Observatory, Casilla 603, La Serena, Chile*
[13]*Department of Physics & Astronomy, University College London, Gower Street, London WC1E 6BT, UK*
[14]*CNRS, UMR 7095, Institut d'Astrophysique de Paris, F-75014 Paris, France*
[15]*Sorbonne Universités, UPMC Univ Paris 06, UMR 7095, Institut d'Astrophysique de Paris, F-75014 Paris, France*
[16]*Kavli Institute for Particle Astrophysics & Cosmology, PO Box 2450, Stanford University, Stanford, CA 94305, USA*
[17]*Laboratório Interinstitucional de e-Astronomia - LIneA, Rua Gal. José Cristino 77, Rio de Janeiro, RJ 20921-400, Brazil*
[18]*Observatório Nacional, Rua Gal. José Cristino 77, Rio de Janeiro, RJ 20921-400, Brazil*
[19]*Department of Astronomy, University of Illinois, 1002 W. Green Street, Urbana, IL 61801, USA*
[20]*National Center for Supercomputing Applications, 1205 West Clark St., Urbana, IL 61801, USA*
[21]*Institut de Ciències de l'Espai, IEEC-CSIC, Campus UAB, Carrer de Can Magrans, s/n, E-08193 Bellaterra, Barcelona, Spain*
[22]*Institut de Física d'Altes Energies, Universitat Autònoma de Barcelona, E-08193 Bellaterra, Barcelona, Spain*
[23]*Institute of Cosmology & Gravitation, University of Portsmouth, Portsmouth PO1 3FX, UK*
[24]*Excellence Cluster Universe, Boltzmannstr. 2, D-85748 Garching, Germany*
[25]*Faculty of Physics, Ludwig-Maximilians University, Scheinerstr. 1, D-81679 Munich, Germany*
[26]*Department of Physics and Astronomy, University of Pennsylvania, Philadelphia, PA 19104, USA*
[27]*Jet Propulsion Laboratory, California Institute of Technology, 4800 Oak Grove Dr., Pasadena, CA 91109, USA*
[28]*Department of Physics, University of Michigan, Ann Arbor, MI 48109, USA*
[29]*Universitäts-Sternwarte, Fakultät für Physik, Ludwig-Maximilians Universität München, Scheinerstr. 1, D-81679 München, Germany*
[30]*Max Planck Institute for Extraterrestrial Physics, Giessenbachstrasse, D-85748 Garching, Germany*
[31]*Center for Cosmology and Astro-Particle Physics, The Ohio State University, Columbus, OH 43210, USA*
[32]*Department of Physics, The Ohio State University, Columbus, OH 43210, USA*
[33]*Australian Astronomical Observatory, North Ryde, NSW 2113, Australia*
[34]*Departamento de Física Matemática, Instituto de Física, Universidade de São Paulo, CP 66318, CEP 05314-970, São Paulo, SP, Brazil*
[35]*George P. and Cynthia Woods Mitchell Institute for Fundamental Physics and Astronomy, and Department of Physics and Astronomy, Texas A&M University, College Station, TX 77843, USA*
[36]*Department of Astronomy, University of Michigan, Ann Arbor, MI 48109, USA*
[37]*Institució Catalana de Recerca i Estudis Avançats, E-08010 Barcelona, Spain*
[38]*Department of Physics and Astronomy, Pevensey Building, University of Sussex, Brighton BN1 9QH, UK*
[39]*Centro de Investigaciones Energéticas, Medioambientales y Tecnológicas (CIEMAT), E-28040 Madrid, Spain*
[40]*Instituto de Física, UFRGS, Caixa Postal 15051, Porto Alegre, RS 91501-970, Brazil*
[41]*Department of Physics, Stanford University, 382 Via Pueblo Mall, Stanford, CA 94305, USA*

This paper has been typeset from a TEX/LATEX file prepared by the author.